GEOPHYSICS, VOL. 64, NO. 4 (JULY-AUGUST, 1999); P. 1181–1192, 10 FIGS., 1 TABLE.

Azimuthal variation in *P*-wave signatures due to fluid flow

Colin MacBeth*

ABSTRACT

The favored dominant mechanism for attenuation in the upper crust at seismic frequencies is intracrack fluid flow. In cracked media, the azimuthal attenuation of the *P*-wave amplitudes arising from such flow is predicted to be quite substantial. The consequence of this variation in azimuth is a modification in the amplitude behavior of the base event from a cracked reservoir due to transmission through the attenuative layer. Indeed, the effect is of sufficient strength to exacerbate, diminish, or reverse variations that arise solely due to the reflectivity coefficient. Thus, although this attenuation is always greatest perpendicular to the crack strike, the direction of the dimming or brightening of the base reservoir event will depend upon the exact attenuation law and the crack properties. The combination of these factors contributes to a wave behavior that can provide a more adequate discrimination between conditions of brine and oil fill than an interpretation assuming the reflection coefficient alone. Unfortunately, regions of commonality do remain, and the distinction between fills is still only apparent for particular reservoir and crack conditions. The attenuated amplitudes are large enough to be seen at small offsets and may possibly account for the significant azimuthal variations in the *P*-wave signatures observed in field data.

INTRODUCTION

During the discussion period of the workshop on Azimuthal Variations in Seismic Signature (held in conjunction with the 1997 SEG Annual Meeting), the subject of attenuation, or more specifically *Q*, was raised in the context of azimuthal variations in the *P*-wave amplitude and fracture-induced (azimuthal) anisotropy. It was noted that azimuthal variations in amplitude and frequency content had in fact been observed in transmission through the overburden using vertical seismic profiles (VSPs) (Horne and MacBeth, 1997) and in the laboratory work of Rathore et al. (1995) for synthesized cracked, saturated sandstone specimens. In addition, systematic effects also have been demonstrated in surface seismic data shot over naturally fractured gas reservoirs (Lynn and Beckham, 1998). The predominant characteristic of all these observations is a greater *P*-wave attenuation in a propagation direction perpendicular to the fracture strike [with Horne and MacBeth (1997) noting some distinct exceptions to this trend]. These observations excite interest as they suggest a link between the anisotropy of a flow (production) process and attenuation anisotropy. This is important as fractures, cracks, or aligned pore space can produce substantial anisotropy in the fluid flow, with up to several orders of magnitude difference in the directions parallel and perpendicular to the strike direction. The flow anisotropy is also large for sandstone crossbeds (Pickup et al., 1994). Thus, whereas fractures or bedding may give rise to weak or moderate anisotropy in the elastic moduli (a few percent in sandstones, 5–30% in limestones), the attenuation anisotropy arising due to the system's flow could be much larger.

To complete the workshop discussion, the above findings were discussed in the context of various published fluid flow mechanisms. Indeed, there are several theories in existence which may furnish an exact mathematical relationship between the fracture geometry, permeabilities, tortuosities, and physical properties of pore fluids and the attenuation. Some of these models have relevance to the seismic bandwidth, but appear to offer conflicting azimuthal behavior in the wave amplitudes. Others do not appear to be important at seismic frequencies. Given the overall significance attached to the subject of fluid flow and attenuation, it is therefore appropriate to discuss attenuation, attenuation mechanisms, and their possible seismic effects as part of these workshop proceedings.

First, I provide a general review of attenuation and mechanisms. Then, I introduce a theoretical framework for treating fracture or crack-related effects that is later adapted to include moduli for flow anisotropy. Finally, modeling assists examination of the likely prevalence of the effects in the setting of hydrocarbon reservoirs surveyed with offshore streamer acquisition. The discussion concentrates on published crack-related effects, but is sufficiently general to also include fractures or aligned pore space. In this context, the word "cracks" is used

Published on Geophysics Online March 16, 1999. Manuscript received by the Editor February 6, 1998; revised manuscript received January 21, 1999.
*British Geological Survey, Murchison House, West Mains Road, Edinburgh, EH9 3LA, Scotland, United Kingdom. E-mail: cdm@bgs.ac.uk.

throughout to refer to the causative features of the azimuthal anisotropy, with the implicit assumption that these can be used interchangeably with fractures or aligned pore space.

Attenuation and Q

Before proceeding further, the term "attenuation" used in the previous paragraph requires further clarification. In fact, it refers to an overall macrofield effect of amplitude and frequency loss. In the generic use of this term, one should be careful to distinguish effects due to the intrinsic nature of the rocks, scattering from the sedimentary sequence, and the natural wave propagation effect due to spherical divergence. For a single propagating plane wave with no spherical divergence, the attenuation coefficient, $\gamma(\omega)$, defines the loss for a specific field experiment. For each angular frequency, ω, the initial amplitude $A_0(\omega)$ decays according to

$$A(\omega) = A_0(\omega)\, e^{-\gamma(\omega)r}, \tag{1}$$

where r the pathlength and $\gamma(\omega)$ is the attenuation coefficient. Thus, there will be an amplitude loss at each frequency in the seismic data, and this gives a direct measure of the attenuation coefficient. An alternative and much more appropriate measure of subsurface absorption is the Q (or specific attenuation) factor. This is defined as the fractional loss of energy in one cycle of wave motion, and is thus a positive number. It is consequently independent of the acquisition and source bandwidth, and is a direct dimensionless measure of the rock. It is related to the attenuation coefficient by

$$\gamma = \frac{\omega}{2vQ} = \frac{\omega}{2v} Q^{-1}, \tag{2}$$

where v is the phase velocity. Q values are normally quoted by their inverse, in order to maintain direct proportionality to the attenuation coefficient. It can be seen that the consequences of attenuation are a reduction in amplitude with distance travelled for each frequency in the wave. Additionally, the relative amplitude loss measured between frequencies can give an indication of the frequency dependence of Q^{-1}.

The specific attenuation factor may be defined for both the P-waves (Q_P^{-1}) or the shear waves (Q_S^{-1}). From a general perspective, Q^{-1} values of around 0.001 can be considered negligible, whereas 0.01 is fairly typical and 0.1 usually leads to high attenuation. Full details on the above definitions, their significance in the geophysical context, and the expected range of numerical values for a range of different materials and frequencies is in the classic paper of Knopoff (1964). There are in fact very few measurements of Q^{-1} within the seismic frequency band (5–50 Hz) and at hydrocarbon exploration depths. Those that exist are generally the result of VSP analyses (for example, McDonal et al., 1958; Pujol and Smithson, 1991; Tonn, 1991; De et al., 1994; Harris et al., 1997). In these, although there may be agreement with some specific features of the individual lithologies, there is little overall consensus to be drawn. This is due in partly to the notoriously difficult issue of measurement reliability, as well as the separability of scattering and intrinsic Q^{-1} factors. The studies cited give a range of Q_P^{-1} values between 0.01 and 0.1 for sandstones, shales, and basalts, while the Q_S^{-1} measurements are not usually meaningful due to their unreliability.

Some specific fluid flow mechanisms

Attenuation may be caused by a whole gamut of microscopic processes which can be collectively summarized as scattering from inhomogeneities such as cracks, pores, fractures, or fine-layered sequences, and intrinsic attenuation or absorption. The latter category includes crystal defects, crack friction, and grain boundary processes, in addition to a number of different styles of viscous fluid motion between component elements of the saturated or partially saturated rock mass. Each possesses its own particular frequency dependence for Q^{-1}. Currently, it is not possible to assign specific mechanisms to a certain depth range of the earth and across a wide frequency bandwidth, with the exception perhaps being the limited confines of the laboratory. The subject of Q mechanisms, therefore, remains an area of active scientific interest. It does appear, however, that between 100 Hz and 1 MHz, intercrack flow could be important, depending upon the individual crack geometries. Furthermore, at seismic frequencies, there is a favored intrinsic absorption mechanism for the saturated porous rocks in the upper crust: local, viscous intracrack flow.

The local or intracrack mechanism of Mavko and Nur (1979) is particularly important because it appears to be one of the only microscopic mechanisms that predicts a realistic magnitude for the attenuation in upper crystal rocks at seismic frequencies. This local (squirt) flow relies upon the fact that rocks possess a small proportion of flat pores or cracks (so-called soft porosity). The important condition is when these cracks contain a small amount of gas and are thus partially saturated. This permits the liquid that is attached to each crack to flow freely in and out of the gas regions when the pore is compressed upon seismic excitation. This process leads to viscous shearing and high energy dissipation. Only partially saturated pores with a small aspect ratio can contribute to this mechanism, with the present working upper maximum for the aspect ratio being 0.1. Thus, the mechanism is important for low-permeability limestones with a high clay content or clay-rich sandstones. In the limit of complete saturation, flow is stifled, and the attenuation expected to disappear. The whole procedure is very dependent upon the pore fluid and geometry, and also sensitive to the spatial distribution of the wetting and nonwetting fluid phases in the hydrocarbon reservoir. For aligned cracks, the mechanism gives a strong attenuation when waves propagate perpendicular to the crack strike (Akbar et al., 1993). The attenuation anisotropy increases with crack radius and the decrease of frequency and saturation. As expected, dissipation from pure shear distortion of the pores is negligible for this mechanism. For rocks containing groups of crack and pore families with different aspect ratio distributions, there is a mixture of squirt flow mechanisms with different time constants.

Another fluid-flow mechanism discussed during the course of this workshop was that of Gelinsky and Shapiro (1995). It is likely to be a dominant cause of attenuation in the sonic log and cross-well kilohertz range, but not in the seismic frequency range. This uses Biot theory as a framework for investigating global flow in a homogeneous, liquid-saturated porous rock. Global flow is defined as the average relative motion between the solid and the viscous pore fluid. Here, the pore shape and local flow are lumped into a single parameter. In this model, an anisotropic, poroelastic rock frame is combined with an anisotropic flow defined by a prespecified

permeability tensor incorporated in the Biot theory. Both the permeability and the elasticity are assumed to possess TIH symmetry (transverse isotropy with a horizontal symmetry axis), thus implying fractures as an underlying causative mechanism. Gelinsky and Shapiro (1995) conclude that, at seismic frequencies, velocity anisotropy must be dominated by the rock frame, whereas the attenuation anisotropy is strongly influenced by the permeability. Both P- and shear-waves are influenced by the permeability-induced dissipation process, and exhibit attenuation and a concomitant velocity dispersion. These effects are characterized by being greatest when parallel to the fracture strike (direction of greatest permeability). Interestingly, due to the way the frequency dependence of this mechanism is formulated, the direction for the maximum attenuation actually switches to the fracture normal at higher (kilohertz) frequencies. Therefore, at such high frequencies, the shear waves have the largest attenuation, the velocity anisotropy is now more affected by the permeability, and the fracture tortuosity and porosity begin to play a significant role in the overall attenuation behavior which becomes increasingly less directional. At frequencies between 1 and 100 Hz, the attenuation is controlled by two characteristic time constants directly related to the fluid viscosity and fracture permeabilities. These constants are very small for crustal rocks containing hydrocarbon fluids. As a consequence, despite being strongly directional, the absolute attenuation is insignificant at these lower (seismic) frequencies. Indeed, such Biot-inherent attenuation may be several orders of magnitude below that predicted for the local flow mechanism, especially in low-permeability rocks (Dvorkin and Nur, 1993).

A third and reemerging set of mechanisms is that of interpore fluid communication. Here, it is visualized that the pore fluid can be squeezed by the incoming stress field from select smaller aspect ratio pores into volumes that are less compliant. Hudson et al. (1996a) investigated this by considering three possible scenarios: flow between individual aligned cracks, flow between nonparallel families of cracks, and flow between the cracks and an equant porous matrix. To simulate these phenomena, previously isolated cracks are perceived to be connected by mechanically invisible fluid pathways that have no effect on the overall properties. The shape and size of these interconnections are not specified so that the pressure relaxation process can be generalized for either neighbouring cracks or the porous network. The mechanisms give a directional attenuation, with the greatest being perpendicular to the crack strike at all frequencies. This response is similar to that predicted by Mavko and Nur (1979), but orthogonal to that predicted by Gelinsky and Shapiro (1995) at seismic frequencies. For seismic frequencies and the physical conditions of most hydrocarbon reservoirs, the process of flow between the aligned Hudson cracks is calculated to be ineffective, and they remain isolated. For the remaining two mechanisms, it appears that the fluid can totally equilibriate with every cycle of the wave motion. This relaxed state is also predicted by Thomsen (1995) for flow between cracks and an equant porosity. It should be noted that the complexity of interflow between crack families means that more specific information is required before a firm conclusion can be reached. However, it does appear that the above mechanisms, when operating within the confines of the theory, cannot yet reproduce a realistic attenuation in the seismic frequency band.

What follows in this paper will focus on both intercrack and intracrack flow as possible causes of attenuation, defining a generic framework for their implementation. Before examining the processes and their effect on the seismic waves, the crack-related stiffnesses must first be considered.

ELASTIC STIFFNESSES AND THEIR RELATION TO FLUID FLOW

Elastic stiffnesses for crack-related anisotropy

A weak concentration of cracks or thin pores in an otherwise isotropic matrix generally weakens the rock, and hence reduces the background elastic stiffnesses, $\mathbf{c}_b$, by amounts proportional to the crack/fracture porosity ϕ_c. These elastic constants, with the resultant first order perturbation can be written in the generic form,

$$\mathbf{c} = \begin{pmatrix} (\lambda+2\mu)(1-e_n) & \lambda(1-e_n) & \lambda(1-e_n) & 0 & 0 & 0 \\ \lambda(1-e_n) & (\lambda+2\mu)\left(1-\zeta^2 e_n\right) & \lambda(1-\zeta e_n) & 0 & 0 & 0 \\ \lambda(1-e_n) & \lambda(1-\zeta e_n) & (\lambda+2\mu)\left(1-\zeta^2 e_n\right) & 0 & 0 & 0 \\ 0 & 0 & 0 & \mu & 0 & 0 \\ 0 & 0 & 0 & 0 & \mu(1-e_t) & 0 \\ 0 & 0 & 0 & 0 & 0 & \mu(1-e_t) \end{pmatrix}, \tag{3}$$

where λ and μ are the Lamé constants and $\zeta = 1 - 2V_S^2/V_P^2$. This expression, in fact, can simulate any one of a variety of crack, pore, or fracture styles, ranging from a volume distribution of intergranular or intragranular cracks (Hudson, 1980, 1981) to the surface distributions of large-scale shear fractures, joints with interlocking rugose surfaces, or even natural fractures with varied gouge conditions (Schoenberg and Sayers, 1995; Hudson et al., 1996b). Clearly, such generalization also implies that it may not be possible to tell details of the shape, texture, or fill without recourse to further (hard) information. Due to this, the results below are considered applicable to cracks, fractures, or even aligned pore volume. The dimensionless scalar fracture indices e_n and e_t are directly proportional to the crack porosity ϕ_c and also related to the respective normal and tangential boundary conditions for incident stress on the fracture faces. These indices are a measure of the stiffness of the background material relative to the crack. For a planar fracture, the indices can be visualized as the ratio of excess compliance due to the

fracture and the background matrix compliance (Schoenberg and Sayers, 1995). The smaller these quantities, the stiffer (or less compliant) the cracks. Cracks may stiffen either due to the material fill or due to an increase in aspect ratio. The exact relationship between fill and geometry depends upon the type of crack. As a specific numerical example, consider a volume distribution of unconnected, small aspect-ratio cracks. The quantity e_n can be partitioned into the porosity, ϕ_c, and the boundary condition terms, b_n and b_t. Thus,

$$e_n = \phi_c b_n \tag{4}$$

and

$$e_t = \phi_c b_t. \tag{5}$$

Clearly these equations lead to another inherent ambiguity in the interpretation of the crack properties, as different combinations of crack porosity ϕ_c and b_n or b_t may yield the same overall value for the perturbation. An additional constraint, therefore, is required to determine these quantities individually, indicating a possible role for core or log analysis. The porosity ϕ_c for an ellipsoidal crack geometry is given by $\frac{4}{3}n\pi\alpha a^3$, where α is the aspect ratio (minor axis divided by major axis), a the mean radius, and n the number per unit volume. The boundary conditions depend on the nature of the cracks and their fill, with the index b_n differentiating between gas fill

$$b_n^{gas} = \frac{1}{\pi\alpha\eta(1-\eta)}, \tag{6}$$

where $\eta = V_S^2/V_P^2$, and liquid fill, for which

$$b_n^{liq} = \frac{b_n^{gas}}{1+\eta_n b_n^{gas}}, \tag{7}$$

where $\eta_n = \rho_{liq}V_{liq}^2/\rho V_P^2$. The index b_t is common to both a gas or liquid fill

$$b_t^{fluid} = \frac{4}{\pi\alpha(3-2\eta)}. \tag{8}$$

The single perturbation term in equation (3) is valid provided the error introduced by omission of the consecutive higher order terms is negligible. A second-order contribution arises due to crack-crack interactions, and the restriction to the single scattering theory will lead to loss of accuracy. The onset of this term provides an upper useable limit of the theory. The formulation has been critically examined for its limits in aspect ratio by Douma (1988) using direct comparison with another theory which deals with larger aspect ratios. The general conclusion for velocity anisotropy of up to 5% is that the single term is valid if aspect ratios are less than 0.3, whether filled with liquid or gas. This gives an upper limit on e_n of approximately 0.25. For cracks, the onset in the growth of the second-order term may also be judged from the expression of Hudson (1980), who quotes the next term in the expansion in number density. This second-order term may be included in equation (3) by the substitutions

$$e_n \rightarrow e_n - 0.6e_n^2 \tag{9}$$

and

$$e_t \rightarrow e_t - 0.5e_t^2 \tag{10}$$

when $\eta = 1/4\,(V_P/V_S = 2)$. This second term becomes important when the error due to the original first-order perturbation rises to some unacceptable value. The error in the phase velocity is 5% when e_n is 0.16, and 10% when e_n is 0.30, with the latter probably being the objective limit of acceptable error. The limit may also be considered from the perspective of Schoenberg and Sayers (1995), in which e_n can be replaced by the exact term $(\lambda+2\mu)Z_N/(1+(\lambda+2\mu)Z_N)$, where Z_N is the excess fracture compliance. The phase velocity error involved in approximating this by the first term in the expansion for small compliance, $Z_N(\lambda+2\mu)$, can be calculated to be 10% when $Z_N(\lambda+2\mu)$ is 0.20, and 15% at 0.30. The limits for the above approach are thus similar, and the final limit of 0.30 is retained for e_n and also e_t in the present work. Outside this limit of validity for the theory, the results are not considered meaningful, and an educated guess as to the behavior is required. For further consideration of a full range of fill conditions, the above constraints permit use of aspect ratios of 0.1 up to a porosity of 2%; for aspect ratios of 0.01 and 0.001, the maximum porosities are set at 0.05% and 0.5%, respectively.

Figure 1 gives values of e_n for different crack porosities up to the limiting values defined above. The curves are calculated using equation (7) for a continuous range of fill conditions from total gas saturation to oil and then brine. The cracks are defined for specific aspect ratios and also for the backgrounds of chalk and sandstone. Table 1 gives the properties of the rocks and fluids used in constructing this plot, which are typical of the UK North Sea. The demarcation between lighter and heavier oils is based on the results quoted for most produced oil according to Batzle and Wang (1992). That work suggests that a density range of 0.75–0.85 g/cm^3 together with a velocity range of 1.15–1.35 km/s is most appropriate. Figure 1 defines the ability to discriminate different crack conditions on the basis of e_n measured from the seismic data using the velocity or reflected amplitudes. One common feature is the more rapid change in e_n as the gas-saturated condition is approached. This is due to the sudden reduction in crack stiffness. Thus, reservoirs where the hydrocarbon is stored in low porosity, thin ($\alpha = 0.001$) aspect-ratio voids remain seismically indistinguishable from brine fill until the onset of the gas phase. There is less sensitivity when comparing the oil-filled and brine-filled conditions with those for different aspect ratios, which leads to a difficulty in distinguishing these particular fills. The effect of increased porosity would be to scale these overall results, but not alter the conclusions significantly. The value of b_t remains constant with fill, but varies with aspect ratio, and thus cannot be used to distinguish fill type for these fluids.

The framework in equation (3) must now be extended to incorporate the contribution of attenuation. This is the subject of the next section.

Table 1. Elastic properties of rocks and liquids used in the calculations.*

	V_P (km/s)	V_S (km/s)	ρ (g/cm^3)
Brine	1.71	—	1.10
Live oil	1.15	—	0.75
Claystone/shale	2.46	1.23	2.30
Sandstone	3.08	1.54	2.25
Chalk	3.62	1.81	2.42

*The rock properties are log averages from the UK central North Sea. The brine and oil properties are computed from Batzle and Wang (1992) for a reservoir pressure of 38 MPa and a temperature of 112°C (MacBeth et al., 1997). The salinity of the brine is 150 000 ppm.

How does fluid flow affect the crack-related stiffnesses?

The general effect of the process of dissipation may be included in the stress-strain relations by using complex, frequency-dependent elastic moduli. The exact form of the frequency dependence depends upon the equations of motion for the underlying mechanism. Knopoff (1964) reviews many of the possible models and their resultant frequency dependence. Here, a specific set of models is considered with their basis in the theory for predicting the overall properties of cracked media. This leads ultimately to a simple, but general, expression for crack-related attenuation.

The effect of fluid flow is to alter only b_n, and hence e_n. This neglect of e_t appears natural, as diffusion of pressure is equivalent to the presence of damping under compression for the material within the crack. Indeed, it can be assumed that because the shear stress applied to the crack face does not give rise to a volume change, b_t should be unaffected to first order. Such reasoning is applicable to the work of Mavko and Nur (1979) and the similar partially saturated intracrack model of Hudson (1988), together with Hudson et al. (1996a) and Thomsen (1995) for intercrack diffusion models. The models all allow for a pressure relaxation at some limited distance. The effect can be effectively categorized by casting the different mechanisms into a generalized function for the crack-related flow. The form suggested is identical to equation (7) for different fill types, but with the substitution

$$\eta_n \rightarrow \eta_n/(1+\tilde{z}(\omega)), \tag{11}$$

where $\tilde{z}(\omega)$ is a complex, frequency-dependent quantity that depends upon the particular mechanism. This form assumes that there is one dominant mechanism and hence one distinct time constant. The function $\tilde{z}(\omega)$ must also possess a certain asymptotic behavior, or be defined only within a specific range of frequencies. At high frequencies, there is insufficient time in each cycle of wave motion to permit pressure equalization, and hence the fluid moves relatively little. As a consequence, the fluid may be regarded as isolated in the cracks or portion of the crack volume. In this unrelaxed state, $\tilde{z}$ must be zero, because equation (7) then yields the result for isolated, liquid-filled cracks. For lower frequencies, the seismic waves have sufficient time during the cycle of the wave to establish pressure equalization, and the saturated rock again acts as an elastic solid. Compensation for the relaxed fluid phase renders the rock more compliant. In this relaxed state, $\tilde{z}$ should be very large, with equation (7) returning the result for totally compliant (gas-filled) cracks. The way in which the transition from a relaxed to an unrelaxed state is made depends on the specific frequency dependence of $\tilde{z}$ which, in turn, depends upon the flow mechanism. The nature of the transition between one extreme and the other is essential to the understanding of seismic attenuation and is the feature of principal concern in attenuation studies. A natural addition to the representation in equation (11) may also be considered from the compliance approach of Schoenberg and Sayers (1995), by defining a complex fracture compliance $\tilde{Z}_N$. This could account for the difference in fluid flow parallel and across the fracture planes. An exact relationship for $\tilde{Z}_N$ is the subject of future work.

With the general form for the treatment of flow in place, a specific attenuation law is now assessed for its impact on the seismic wavefield properties.

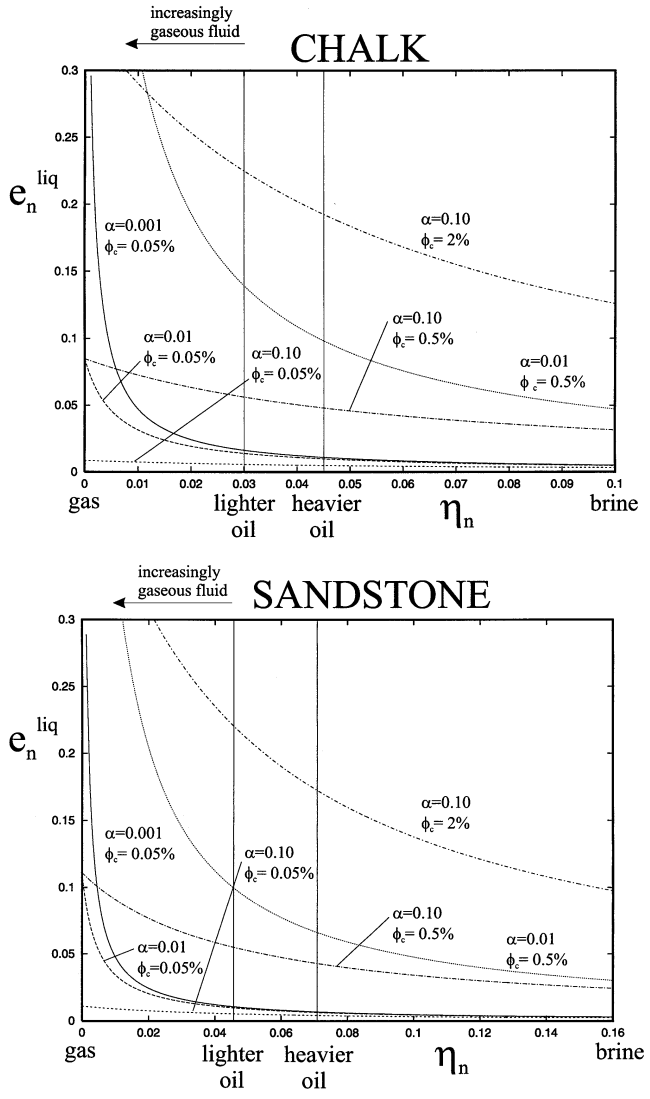

FIG. 1. Variation in crack stiffness for continuously changing fill parameter η_n ($=\rho_{liq}/V_{liq}^2/\rho V_P^2$) and different aspect ratios (α). The vertical lines demarcate conditions appropriate to most produced hydrocarbons according to Batzle and Wang (1992). The other crack index, e_t^{liq}, is invariant with fill. Different crack porosities, ϕ_c, are considered, with the largest being the upper limit using the theory in this paper.

EFFECTS ON SEISMIC DATA

Frequency dependence of phase velocity and attenuation

The complex fracture index, $\tilde{e}_n = e_n^R + ie_n^I$, determined from the above, results in complex elastic constants $\tilde{\mathbf{c}}$. The velocity anisotropy is influenced through the real part, e_n^R, and the angle-dependent attenuation through the imaginary part, e_n^I. The effect of each may be assessed by examining the propagation of a homogeneous plane P-wave. The wave properties arising from complex elastic constants can be determined using the same formulations as the elastic case by inserting the solution

$$\mathbf{u} = \hat{\mathbf{u}}\, e^{-i\omega \mathbf{p}\cdot\mathbf{r}} \tag{12}$$

into the equation of motion, where **u** is the displacement vector, **p** the slowness, and **r** the distance and direction of travel. For an anisotropic medium, this leads to the Kelvin-Christoffel equation, which in general can now only be satisfied by introducing complex phase slowness $\tilde{\mathbf{p}}$, where

$$\tilde{\mathbf{p}} = \mathbf{p}_R + i\mathbf{p}_I. \tag{13}$$

It follows that the wave must attenuate according to $e^{-\omega p_I r}$ for a distance r along each specific phase direction. The attenuation factor, $\gamma(\omega)$, is given by ωp_I and hence $Q^{-1}(\omega)$ by $2p_I/p_R$ from equation (2) above. To illustrate the impact of the crack-related term arising from $\tilde{z}(\omega)$, the specific case of partial saturation or squirtlike flow is chosen (Hudson, 1988) as it is easy to implement. For this, equation (6) includes the relationship

$$\tilde{z}(\omega) = \frac{1 - i\omega\tau}{i\omega\tau}. \tag{14}$$

The relaxation period, τ, depends upon fluid viscosity, fluid saturation, crack geometry, and fill. However, because a suitable estimate of fluid saturation must be guessed, a value for τ of 40 ms is chosen as it gives a significant result in the seismic band. This will not significantly alter the overall conclusions of this present work, and it provides an opportunity to examine the interplay between crack geometry and fill. Figure 2 shows the resulting $Q_{//}^{-1}$ for horizontal propagation parallel to the fracture strike. Here, the maximum porosity limits for each crack aspect ratio more restricted than in Figure 1; otherwise, the range in behavior calculated in later sections becomes too large to plot satisfactorily. These limits are now maintained throughout this current work. The calculations are for three different aspect ratios and for both oil and brine fill. The peak moves to lower frequencies with smaller aspect ratios and change from oil to brine fill, while the maximum value varies only slowly with these conditions. Thus, within the seismic bandwidth, the smaller aspect ratio cracks are less dissipative. Figure 3 shows the corresponding velocity dispersion. The velocity ranges gently between the value for total gas (low-frequency result) and that for total liquid fill (high frequency). The peak in the attenuation lies within the transition zone between these two asymptotes, where most of the energy is lost during each wave cycle.

Directional dependence of phase velocity and amplitude

Attenuation of the wavefield is examined more directly by inspection of the resultant amplitudes. For horizontal wave propagation, for which the attenuation effects are largest, the ratio of the amplitudes parallel and perpendicular to the fracture strike is

$$\frac{A_\perp}{A_{//}} = e^{-(\gamma_\perp - \gamma_{//})r}, \tag{15}$$

where the attenuation factors parallel $\gamma_{//}$ and perpendicular $\gamma_\perp$ to the crack strike are given by

$$\gamma_{//} = \frac{\omega}{\mathrm{Im}\left[1 - \zeta^2 \tilde{e}_n\right]^{1/2} V_P} \tag{16}$$

and

$$\gamma_\perp = \frac{\omega}{\mathrm{Im}[1 - \tilde{e}_n]^{1/2} V_P}, \tag{17}$$

where V_P is the background isotropic velocity. A formula for the general directional behavior in nonsymmetry planes is given in Appendix A. The amplitude ratio in equation (15) is calculated numerically for path lengths of 300, 400, and 500 m through the cracked, dissipative medium, and for different aspect ratios and fills in Figure 4. There are marked differences in the amplitude decay with aspect ratio, which relate directly to the movement of the attenuation peak in Figure 2. However, brine and oil are difficult to resolve for small (0.001) and large (0.1) aspect ratios, but values of 0.01 provide an amplitude reduction from 0.7 (brine) to 0.4 (oil). As expected, there is a rapid change near gas saturation, where the amplitude ratio is unity. It is important to note that the velocity anisotropy corresponding to these results is actually no more than 5%. The results can therefore explain most of the VSP observations in Horne and MacBeth (1997) as arising from a weakly anisotropic but saturated, porous overburden. The effect on the transmitted wavefield for this case is illustrated in Figure 5

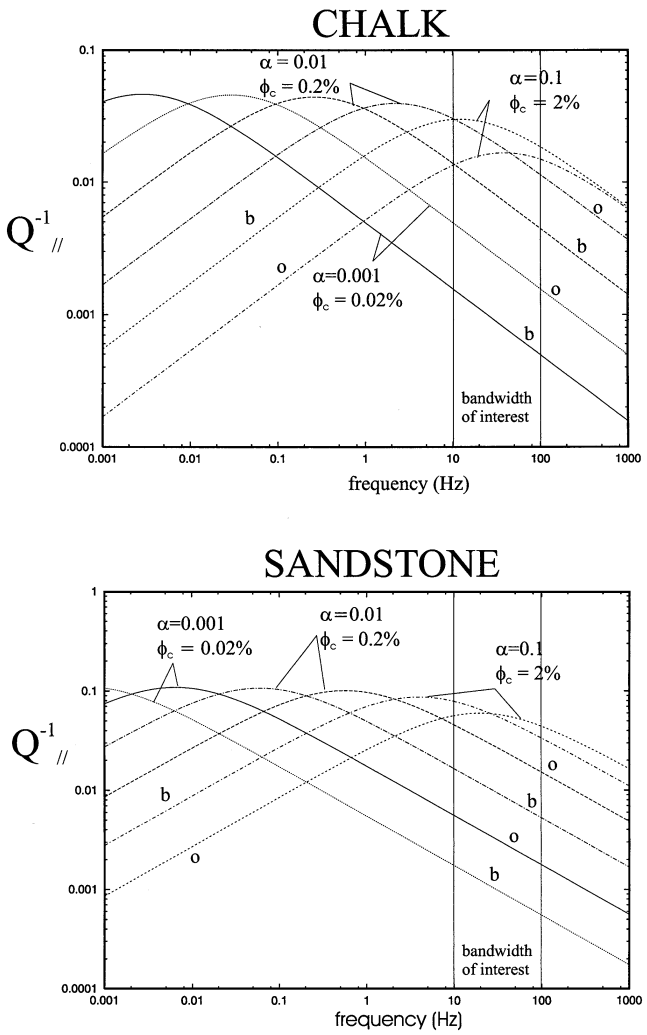

FIG. 2. Dimensionless $Q_{//}^{-1}$ factor for horizontal propagation parallel to the crack strike. Curves are for oil (o) and brine (b) fill, and also different aspect ratios α. Brine moves the peaks to lower frequencies, so too does a reduction in aspect ratio. Curves are based on the attenuation law defined in equation (14), with a characteristic time constant of 40 ms.

for a wavelet of 30-Hz peak frequency, an amplitude ratio of approximately 0.5 being predicted. The results in Figure 4 are also in qualitative agreement with the laboratory work of Rathore et al. (1995), which gives a very large amplitude ratio for inclusions with an aspect ratio of 0.004.

Directional dependence of reflected *P*-wave amplitudes

Directional amplitude variations have been observed in surface seismic data both onshore (Lynn et al., 1996; Mallick et al., 1996) and offshore (MacBeth et al., 1997). Such variations have been largely attributed to changes in the reflection coefficient at a specific interface, although recent work by Lynn and Beckham (1998) suggests attenuation as a possible contributary factor. In light of these observations, it is important to understand how attenuation may influence the azimuthal variation of the *P*-wave amplitude for reservoir conditions. To examine this, two typical UK North Sea scenarios are considered: a fractured chalk overlying a sandstone and capped by a claystone overburden, and a fractured sandstone encased in claystone. The former case gives a distinct high-impedance step, whereas the latter forms a medium contrast. The elastic properties for these models are determined by averaging logs from the central North Sea used for previous work (MacBeth et al., 1997; Ohlsen et al., 1998). These isotropic background properties are shown in Table 1.

Figure 6 shows the results from numerical computation of the reflection coefficients for the chalk model. The coefficients are calculated for an angle of incidence corresponding to the maximum offset delivered by acquisition using a standard 3-km towed streamer. They simulate the amplitude that would be recorded in a fixed offset azimuthal gather when parallel and perpendicular to the crack strike. Raybending is simulated initially for the bottom chalk coefficient by increasing the incidence to 38° and reducing the incidence at the top chalk to

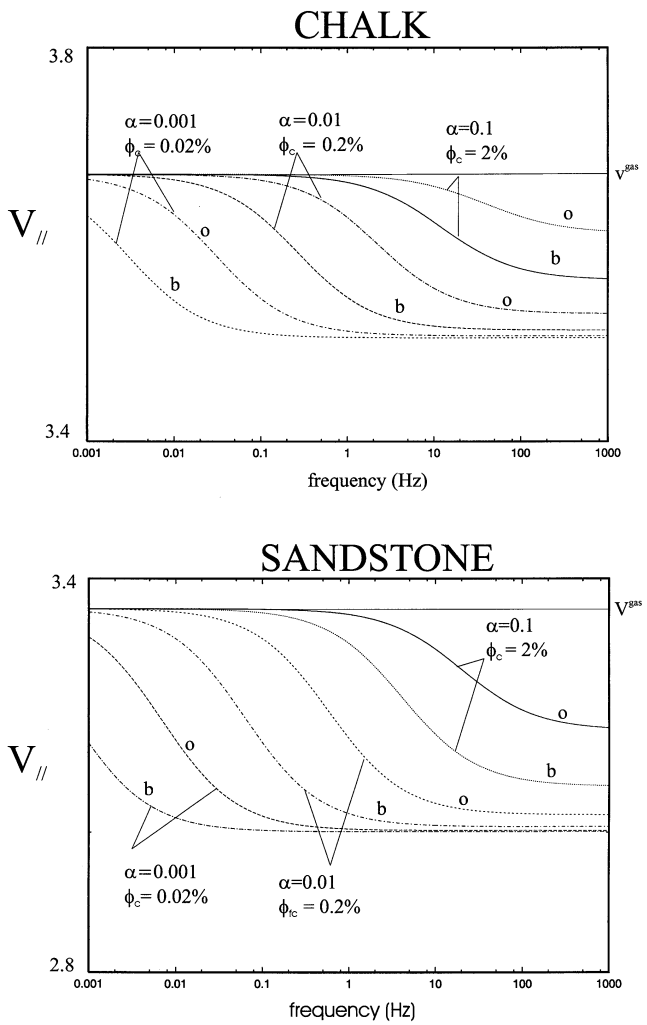

FIG. 3. Velocity dispersion corresponding to Figure 2, for oil-filled (o) and brine-filled (b) cracks, and different aspect ratios α. Oil moves the curves to lower frequencies, so too does a reduction in aspect ratio. V^{gas} is the velocity for completely gas-saturated cracks.

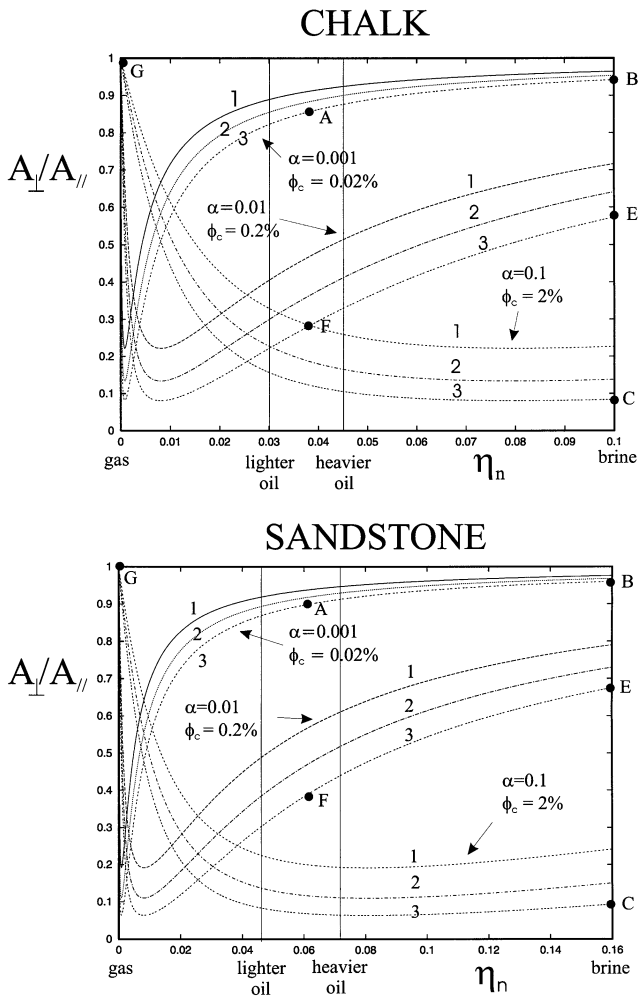

FIG. 4. Ratio of amplitudes perpendicular and parallel to the crack strike for horizontal wave propagation and the attenuation mechanism proposed in equation (14). Calculations are for a frequency of 30 Hz and range of fluid fills defined by the parameter η_n ($=\rho_{liq}V_{liq}^2/\rho V_P^2$). Numbers indicate pathlengths: 1—300 m, 2—400 m, 3—500 m. Labelled filled circles correspond to points in this plot chosen for later synthetic seismogram modeling.

28°. The figure plots the ratio of reflected amplitudes perpendicular and parallel to the fracture strike as a function of crack conditions for both the top and bottom chalk. For the thinnest cracks, for which e_n remains small until the onset of gas saturation (see Figure 1), the top and bottom chalk reflections lead to a brightening perpendicular to the crack strike with brine and various oil fills. However, totally gas-saturated cracks are likely to lead to a dimming perpendicular to the crack strike. On the other hand, larger aspect ratios of 0.1 (larger e_n values) will produce a dimming perpendicular to the crack strike if there is sufficient porosity. Aspect ratios of 0.01 and 0.1 (for low porosities) appear to give little variation with crack fill for this model. The overall bottom chalk response is similar to the top chalk, but the depth of the variation is greater. In all the cases, both reflection coefficients retain the same sign. The above conclusions are not significantly altered for the sand model, except for the largest aspect ratio and porosity for which the dimming is replaced by a brightening with brine fill, followed by a progressive change to a dimming at the gas fill. It should be noted that the above effects are model dependent. Analyses of further models are offered by Sayers and Rickett (1997) for the classified amplitude variation with offset (AVO) response of gas sands. Clearly the disadvantage in interpretation of observations based on the reflection coefficients is that they are small in magnitude. Thus, if the behavior is dominated solely by the reflected amplitudes, it does not provide sufficient discrimination between oil and brine.

To include the influence of ray-bending and wave-propagation effects more exactly, azimuthal trace gathers are calculated using the anisotropic reflectivity method (Taylor, 1991). In this computation, all multiples are included. The source is

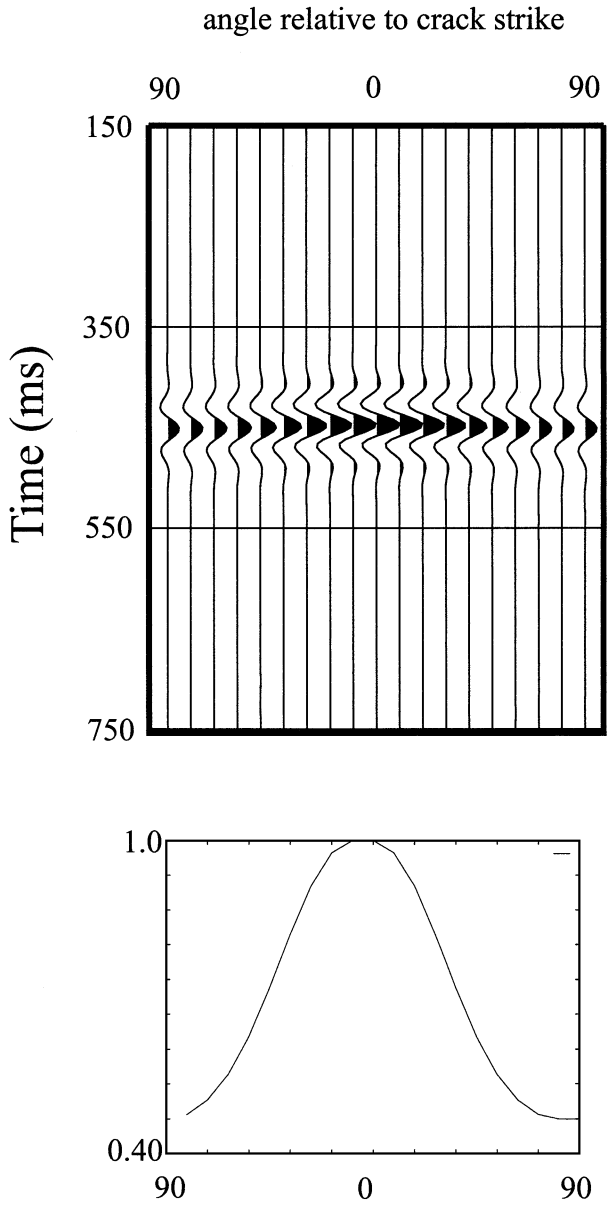

FIG. 5. Synthetic seismogram showing a common receiver gather at 1400 m from an azimuthal VSP with an offset of 700 m. The peak frequency of the wavelet is 30 Hz. Note the strong decrease in amplitude perpendicular to the crack strike. The material is an anisotropic sandstone, the cracks saturated with brine, and the matrix properties given by Table 1. There is a velocity anisotropy of 5%. The lower diagram shows the average amplitude.

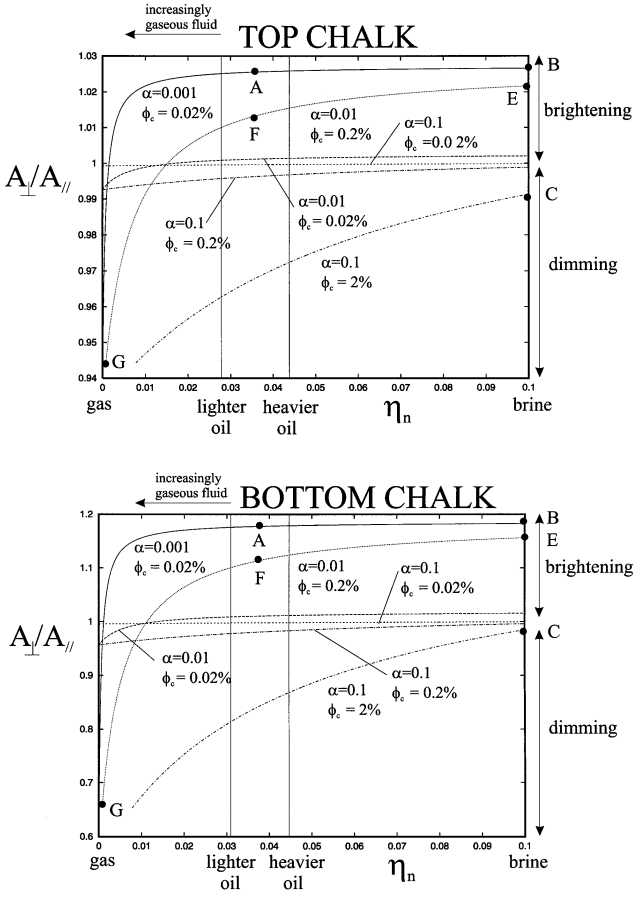

FIG. 6. Ratio of reflected amplitudes perpendicular and parallel to the crack strike for continuous fill variation ($\eta_n = \rho_{liq} V_{liq}^2 / \rho V_P^2$), and different aspect ratios (α) and porosities. Solid circles correspond to points in this plot chosen for later synthetic seismogram modeling.

an explosion, and the hydrophone recording is taken to be the vertical component of motion. For both reservoir models, the conditions of the cracks in these initial calculations correspond to points A ($\alpha = 0.001$, oil fill), B ($\alpha = 0.001$, brine fill), and C ($\alpha = 0.1$, brine fill) in Figures 6 and 7. Figure 8 shows the resultant fixed-offset azimuthal gathers for the chalk model. The average amplitude curves for the top and bottom reservoir events are in good agreement with the reflection coefficient result for the thinnest cracks. These give a brightening perpendicular to the crack strike for both events. For the largest aspect ratio, the top chalk event dims when perpendicular to the crack strike as expected, but the bottom chalk event brightens slightly. This is not predicted by the reflection coefficient calculation and is a consequence of raybending through the chalk. Results for the sand model also agree with this interpretation. However, in this case the top sand events have little overall reduction in amplitude.

To evaluate the influence of crack-related attenuation on this picture of azimuthal variation, the synthetic seismograms are recomputed but with the stiffnesses now becoming complex according to equations (14), (11), and (7). For ease of computation, a frequency independent Q^{-1} is used, corresponding to the value at the wavelet's 30-Hz peak frequency. Attenuation reduces the amplitude of the base event but leaves the top event almost untouched. This is expected, as the complex stiffness substituted into the equations for the reflection coefficient may give rise to small phase changes and alter the absolute value of the reflected amplitude by a small amount. The major influence is through transmission across the reservoir zone. The effect of the chosen attenuation model is to lead to a diminuition of the amplitude perpendicular to the crack strike for all but the total gas-filled case. As the attenuation has a more dramatic effect on the amplitudes than the reflection coefficients (compare the scales for Figure 4 with Figures 6 and 7), the influence is therefore significant. Thus, the attenuation may exacerbate, diminish, or reverse the effect of the reflection coefficient. Figure 8 shows this effect for the chalk model, where a strong dimming perpendicular to the crack strike for the base event now replaces the previous weaker brightening for $\alpha = 0.1$ (C). By contrast, the brightening of the base chalk event is diminished but not reversed for $\alpha = 0.001$ (A or B). The reduced effect for thin cracks is because the attenuation

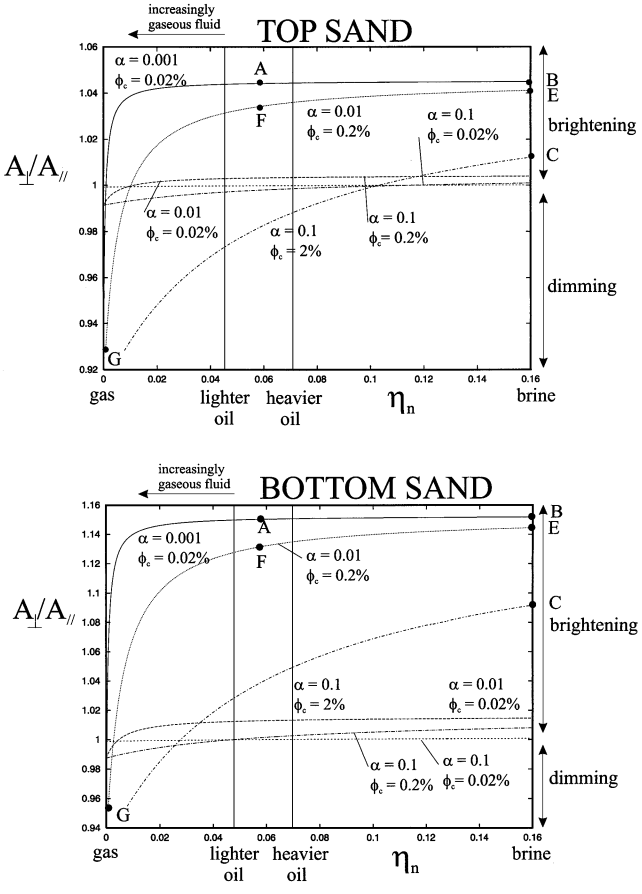

FIG. 7. Ratio of reflected amplitudes perpendicular and parallel to the crack strike for continuous fill variation ($\eta_n = \rho_{liq} V_{liq}^2 / \rho V_P^2$) different aspect ratios (α), and porosities ϕ_c. Solid circles correspond to points in this plot chosen for later synthetic seismogram modeling.

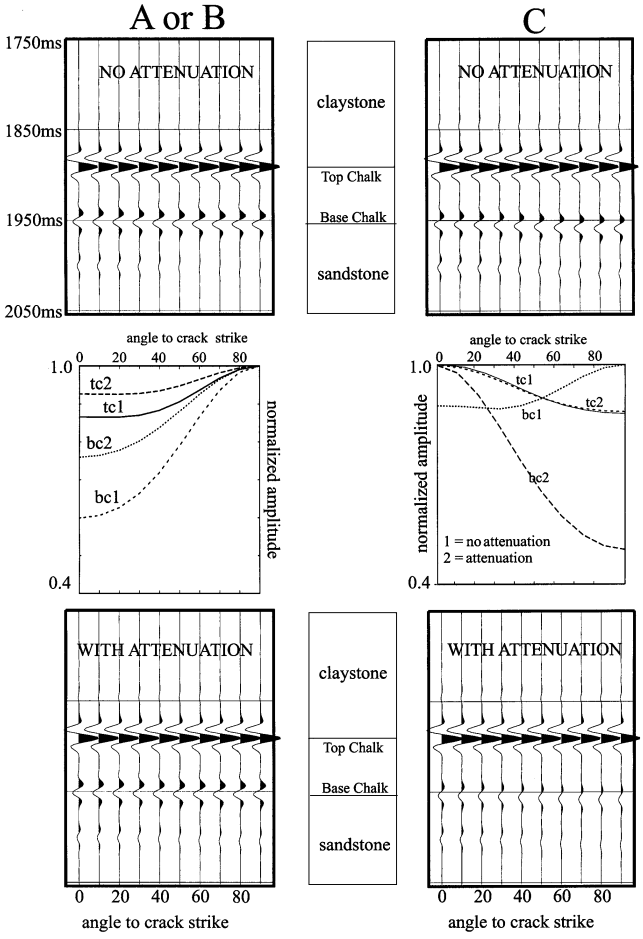

FIG. 8. Synthetic seismograms for a 150-m-thick chalk reservoir, with (bottom) and without (top) crack-related attenuation. Averaged amplitudes for each event are shown in the central diagram, with the top (tc) and base (bc) events. The cracks are brine or oil filled (A or B) with an aspect ratio of 0.001, or brine filled with an aspect ratio of 0.1 (C). The labels correspond to the points in Figures 4 and 6. Seismograms are normalized with respect to the largest amplitude for the top event.

is much weaker in this second case (see Figure 4). The general pattern of this behavior is repeated for the reservoir sand model in Figure 9.

From Figures 8 and 9, the amplitude effects appear complicated, and perhaps difficult to interpret. To examine this further, synthetic seismograms are computed for the chalk model and cracks with an aspect ratio of $\alpha = 0.01$ for gas, oil, and brine fill. The results are shown in Figure 10. These conditions correspond to points E, F, and G in Figures 4 and 6. For points E and F for the top chalk event, the relative reflection coefficient is predicted to be close to unity, and hence there is no response. On the other hand, the gas fill produces a sharp dimming in the reflectivity due to the enhanced compliance (see Figure 1). Inspection of the bottom chalk event shows a more complicated behavior. The brine-filled cracks are expected to show dimming perpendicular to the crack strike due to the attenuation alone. In fact, they show little response due to the competing effects of ray bending. The oil-filled cracks have a larger attenuation and hence exhibit the predicted dimming.

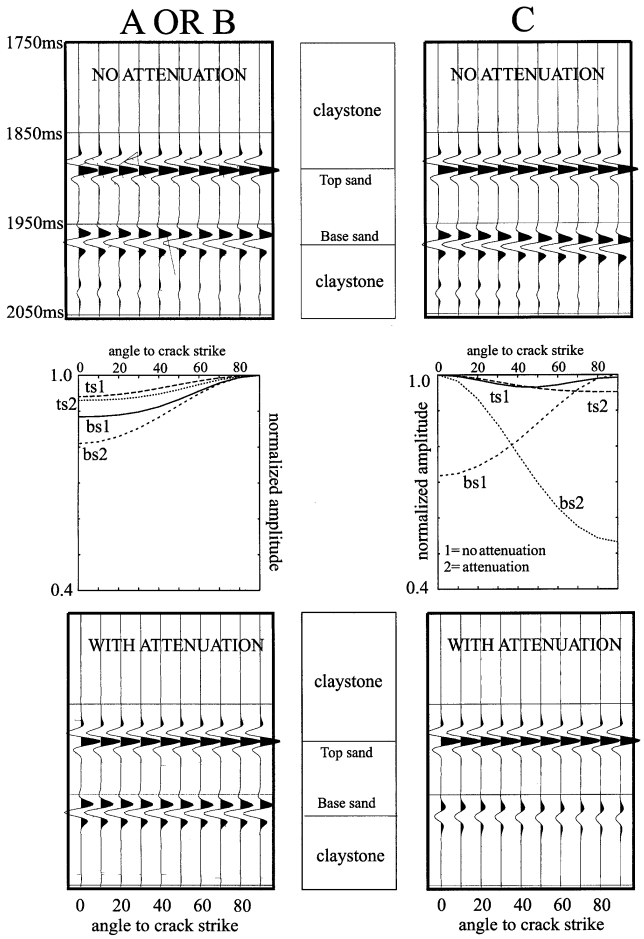

FIG. 9. Synthetic seismograms for a 150-m-thick sandstone reservoir. Averaged amplitudes for each event are shown in the central diagram, and the top (ts) and base (bs) events, with (bottom) and without (top) attenuation. Calculations are for brine- and oil-filled cracks with an aspect ratio of 0.001 (A or B) and brine-filled cracks with an aspect ratio of 0.1 (C). Labels correspond to points in Figures 4 and 7. Seismograms are normalized by the maximum amplitude for the top event.

Finally, gas fill gives no attenuation (no azimuthal variation and an insignificant decay in absolute terms) but a dimming perpendicular to the crack strike due entirely to the reflection coefficient. The three situations are clearly quite distinct, but not necessarily intuitive, and thus interpretation of such effects in data must be strongly model based.

DISCUSSION AND CONCLUSIONS

The effect of crack-related attenuation is surprisingly large, especially when considering that the velocity anisotropy induced in the discussed examples is at most 5%. It is also in general much larger than the amplitude changes due to the reflection coefficient alone. This could explain many of the observed azimuthal variations for base reservoir events, especially when the corresponding theoretical predictions for the reflection coefficients is small. Unfortunately, to confirm this explanation requires an accurate field measurement of the phenomenon. It is also desirable to be able to estimate the frequency dependence of Q^{-1}. Unfortunately, field measurement of attenuation is commonly fraught with difficulties and does not live up to such theoretical expectations. This is generally true regardless of whether the estimates are made in multilevel VSP or using some other wavetype such as surface waves (MacBeth, 1983). This opinion is underlined by the many studies using the familiar spectral ratio technique, which often yield negative values (De et al., 1994). This is also the conclusion of investigations of different estimation techniques (Tonn, 1991). The evaluation of a frequency dependence is even more uncertain (Harris et al., 1997). A partial explanation for these may be sought in the masking effect of other attenuating phenomena, such as geometric spreading and scattering from irregularities and layering. These factors are not easily separated

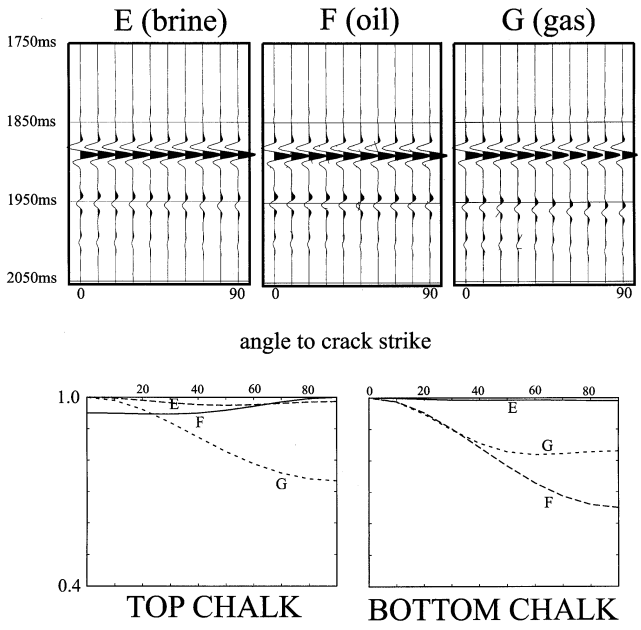

FIG. 10. Synthetic seismograms for a chalk reservoir with cracks possessing an aspect ratio of 0.01 and brine (E), oil (F), and gas (G) fills. The crack conditions correspond to points E, F, and G in Figures 4 and 6. Averaged amplitudes are shown for each event.

in field experiments. There may also be obfuscation by lack of reliability in the seismic acquisition. In this context, it appears a difficult task to extend estimation techniques to surface seismics, although the added information from the azimuthal variation of *P*-wave signatures may well provide a robust approach to determining this information. The work of MacBeth et al. (1997) suggests that an offset-dependent amplitude and wavelet matching procedure may be an appropriate method for analysis. Furthermore, the azimuthal variation of velocity due to the dispersion effects in Figure 3 could also be monitored using interval velocity estimates.

The importance of the intrinsic quality factor, Q^{-1}, is indisputable. Indeed, this rock property has the potential to provide direct access to many processes critical to reservoir evaluation, particularly for time-lapse surveying or monitoring. Before this can be reached, much work still remains on the theoretical side to establish appropriate mechanisms for fluid flow in natural fractures. From the more practical perspective, acquisition must become more reliable.

ACKNOWLEDGMENTS

This work is funded by the sponsors of the Edinburgh Anisotropy Project: Agip, Amerada Hess, Amoco, BG plc, Chevron, Conoco, Elf, Fina, Mobil, PGS, Phillips, Saga Petroleum, Schlumberger, Shell, Texaco, and Veritas DGC. The material is presented with approval from all project partners and the Director of the British Geological Survey.

REFERENCES

Akbar, N., Dvorkin, J., and Nur, A., 1993, Relating *P*-wave attenuation to permeability: Geophysics, **58**, 20–29.

Batzle, M., and Wang, Z., 1992, Seismic properties of pore fluids: Geophysics, **57**, 1396–1408.

De, G. S., Winterstein, D. F., and Meadows, M., 1994, Comparison of *P*- and *S*-wave velocities and *Q*'s from VSP and sonic log data: Geophysics, **59**, 1512–1529.

Douma, J., 1988, The effect of the aspect ratio on crack-induced anisotropy: Geophys. Prosp., **36**, 614–632.

Dvorkin, J., and Nur, A., 1993, Dynamic poroelasticity: A unified model with the squirt and the Biot mechanisms: Geophysics, **58**, 524–533.

Gelinsky, S., and Shapiro, S. A., 1995, Anisotropic permeability: influence on seismic velocity and attenuation, Proc. 6th Internat. Workshop on Seis. Anisotropy, 433–461.

Harris, P. E., Kerner, C., and White, R. E., 1997, Multichannel estimation of frequency-dependent *Q* from VSP data: Geophys. Prosp., **45**, 87–109.

Horne, S., and MacBeth, C., 1997, AVA observations in azimuthal VSPs: 59th Mtg., Eur. Assn. Geosci. Eng., Expanded Abstracts, P051.

Hudson, J. A., 1980, Overall properties of a cracked solid: Math. Proc. Cambridge Phil. Soc., **88**, 371–384.

——— 1981, Wavespeeds and attenuation of elastic waves in material containing cracks: Geophys. J. Roy. Astr. Soc., **64**, 133–150.

——— 1988, Seismic wave propagation through material containing partially saturated cracks: Geophys. J. Roy. Astr. Soc., **92**, 33–37.

Hudson, J. A., Liu, E., and Crampin, S., 1996a, The mechanical properties of materials with interconnected cracks and pores: Geophy. J. Internat., **124**, 105–112.

——— 1996b, Transmission properties of a fault plane: Geophy. J. Internat., **125**, 559–566.

Knopoff, L., 1964, *Q*, Rev. Geophys., **2**, 625–660.

Lynn, H., and Beckham, W., 1998, *P*-wave azimuthal variations in attenuation, amplitude and velocity in 3-D field data: Implications for mapping horizontal permeability anisotropy: 68th Ann. Internat. Mtg., Soc. Expl. Geophys., Expanded Abstracts, 193–196.

Lynn, H. B., Simon, K. M., Bates, C. R., and Van Dok, R., 1996, Naturally fractured gas reservoirs, seismic characterization: 66th Ann. Internat. Mtg., Soc. Expl. Geophys., Expanded Abstracts, 1360–1363.

MacBeth, C. 1983, Propagation and attenuation of seismic Rayleigh waves along single paths in Scotland: Ph.D. thesis, Univ. of Edinburgh.

MacBeth, C., Jakubowicz, H., Kirk, W., Li, X-Y., and Ohlsen, F., 1997, Fracture-related variations with offset and azimuth in marine seismic data: 67th Ann. Internat. Mtg., Soc. Expl. Geophys., Expanded Abstracts, 195–198.

Mallick, S., Craft, K. L., Meister, L. J., and Chambers, R. E., 1996, Computing of principal directions of azimuthal anisotropy from *P*-wave seismic data: 66th Ann. Internat. Mtg., Soc. Expl. Geophys., Expanded Abstracts, 1862–1865.

Mavko, G. M., and Nur, A., 1979, Wave attenuation in partially saturated rocks: Geophysics, **44**, 161–178.

McDonal, F. J., Angona, F. A., Mills, R. L., Sengbush, R. L., Van Nostrand, R. G., and White, J. E., 1958, Attenuation of shear and compressional waves in Pierre Shale: Geophysics, **23**, 421–439.

Ohlsen, F., MacBeth, C., Vestby, J., and Magnus, I., 1998, Fracture estimation from walkaway VSPs recorded in a deviated well: 66th Ann. Mtg., Eur. Assn. Geosci. Eng., Expanded Abstracts, 10–43.

Pickup, G. E., Ringrose, P. S., Jensen, J. L. and Sorbie, K. S., 1994, Permeability tensors for sedimentary structures: Math. Geol. **26**, 227–250.

Pujol, J., and Smithson, S., 1991, Seismic wave attenuation in volcanic rocks from VSP experiments: Geophysics, **56**, 1441–1455.

Rathore, J. S., Fjaer, E., Holt, R. M., and Renlie, L., 1995, *P*- and *S*-wave anisotropy of a synthetic sandstone with controlled crack geometry: Geophys. Prosp., **43**, 711–728.

Sayers, C. M., and Rickett, J. E., 1997, Azimuthal variation in AVO response for fractured gas sands: Geophys. Prosp., **45**, 165–182.

Schoenberg, M., and Sayers, C. M., 1995, Seismic anisotropy of fractured rock: Geophysics, **60**, 204–211.

Taylor, D. B., 1991, ANISEIS V Manual: Applied Geophysical Software.

Thomsen, L., 1986, Weak elastic anisotropy: Geophysics, **51**, 1954–1966.

——— 1995, Elastic anisotropy due to aligned cracks in porous rock: Geophys. Prosp., **43**, 805–830.

Tonn, R., 1991, The determination of the seismic quality factor *Q* from VSP data: A comparison of different computational methods: Geophys. Prosp., **39**, 1–27.

APPENDIX A

DIRECTIONAL DEPENDENCE OF ATTENUATION FOR WEAK ANISOTROPY

For nonsymmetry planes, a formula for the general directional dependence may be determined by adapting Thomsen's (1986) weak anisotropy approximation for a transversely isotropic medium. This can be achieved by replacing the incidence angle for the original TIV (transverse isotropy with a vertical symmetry axis) medium by an angle χ between the phase direction and the horizontal symmetry axis. For a general phase direction specified by azimuth ϕ and incidence θ, this gives $\cos \chi = \cos \phi \sin \theta$. The fracture indices $\tilde{e}_n$ and $\tilde{e}_t$ are related to the complex versions of the weak parameters via

$$\tilde{\epsilon} \approx 2\eta(1-\eta)\tilde{e}_n \tag{A-1}$$

and

$$\tilde{\delta} \approx 2\eta(\tilde{e}n - \tilde{e}t), \tag{A-2}$$

where both e_n^R and e_n^I must now be considered as small. The phase velocity equations for the P-waves can thus be rearranged for slowness

$$\tilde{p} = p_b\left(1 + \frac{\tilde{e}_t}{2}\eta \sin^2 2\chi + \frac{\tilde{e}_n}{2}(1 - 2\eta \sin^2 \chi)^2\right) \tag{A-3}$$

where p_b is the background isotropic slowness. The imaginary part of the slowness is

$$p_I(\chi) = p_b\, e_n^I(1 - 2\eta \sin^2 \chi)^2/2, \tag{A-4}$$

which leads to

$$\gamma(\psi, \theta) = \omega p_b e_n^I(1 - 2\eta \sin^2 \chi)^2/2 \tag{A-5}$$

and

$$Q^{-1}(\psi, \theta) \approx e_n^I(1 - 2\eta \sin^2 \chi)^2. \tag{A-6}$$